

1 **Title: Chloroplasts navigate towards the pathogen interface to counteract**
2 **infection by the Irish potato famine pathogen**

3 **Authors:** Alexia Toufexi^{1†}, Cian Duggan^{*1†}, Pooja Pandey¹, Zachary Savage¹, María
4 Eugenia Segretin³, Lok Him Yuen¹, David C. A. Gaboriau², Alexandre Y. Leary¹,
5 Virendrasinh Khandare¹, Andrew D. Ward⁴, Stanley W. Botchway⁴, Benji C. Bateman⁴,
6 Indranil Pan^{5,6}, Martin Schattat⁷, Imogen Sparkes⁸, Tolga O. Bozkurt^{1*}

7 **Affiliations:**

8 ¹Department of Life Sciences, Imperial College London, UK

9 ²Facility for Imaging by Light Microscopy, NHLI, Faculty of Medicine, Imperial College
10 London

11 ³INGEBI-CONICET, Ciudad Autonoma de Buenos Aires, Argentina

12 ⁴Central Laser Facility, Science and Technology Facilities Council Harwell, UK

13 ⁵Centre for Process systems engineering and Centre for Environmental Policy, Imperial
14 College London, UK

15 ⁶The Alan Turing Institute, London, UK

16 ⁷Martin-Luther-Universität Halle-Wittenberg, Germany

17 ⁸School of Biological Sciences, University of Bristol, UK

18 *Correspondence to: o.bozkurt@imperial.ac.uk

19 †These authors contributed equally

20 **Abstract:** Chloroplasts are light harvesting organelles that arose from ancient
21 endosymbiotic cyanobacteria. Upon immune activation, chloroplasts switch off
22 photosynthesis, produce anti-microbial compounds, and develop tubular
23 extensions called stromules. We report that chloroplasts navigate to the
24 pathogen interface to counteract infection by the Irish potato famine
25 pathogen *Phytophthora infestans*, physically associating with the specialised
26 membrane that engulfs pathogen haustoria. Outer envelope protein, chloroplast
27 unusual positioning1 (CHUP1), anchors chloroplasts to the host-pathogen
28 interface. Stromules are induced during infection in a CHUP1-dependent
29 manner, embracing haustoria and interconnecting chloroplasts, to form dynamic
30 organelle clusters. Infection-triggered reprogramming of chloroplasts relies on
31 surface immune signalling, whereas pathogen effectors subvert these immune
32 pulses. Chloroplast are deployed focally, and coordinate to restrict pathogen
33 entry into plant cells, a process actively countered by parasite effectors.

34 **Introduction:** *Phytophthora infestans* is an oomycete pathogen that causes potato late
35 blight, one of the most historically and economically devastating crop diseases. The
36 pathogen penetrates host cells via haustoria, infection structures that extend from its
37 extracellular invasive hyphae. Haustoria are surrounded by the plant-derived extra-
38 haustorial membrane (EHM), across which effectors secreted by the pathogen
39 translocate inside the host cell (Wang et al., 2017; Whisson et al., 2016, 2007). This
40 interface is key to the success or failure of infection and is therefore targeted by focal
41 immune responses of the plant (Bozkurt et al., 2011; Dagdas et al., 2018; Kwon et al.,
42 2008). Remarkably, despite being continuous with the plasma membrane, there is a
43 stark difference in the biochemical composition of the EHM and the plasma membrane.
44 EHM typically lacks surface localized pattern recognition receptors (PRRs), which
45 activate downstream immune responses through recognition of pathogen associated
46 molecular patterns (PAMPs) (Bozkurt et al., 2015, 2014). Activation of immunity at the
47 cell surface stimulates chloroplasts to shut down photosynthesis, synthesize defence
48 hormone precursors, and generate reactive oxygen species (ROS) (Padmanabhan and
49 Dinesh-Kumar, 2010; Su et al., 2018), suggesting that chloroplasts are committed to the
50 plant defence system. Additionally, chloroplasts produce stroma filled tubules
51 (stromules) that have been implicated in defence (Caplan et al., 2015; Kumar et al.,
52 2018). Pathogens are known to target chloroplasts with effector proteins (de Torres
53 Zabala et al., 2015; Jelenska et al., 2007; Pecrix et al., 2018; Petre et al., 2016).
54 Interestingly, several genes associated with resistance to oomycete pathogens were
55 found to encode chloroplast-localized proteins (Belhaj et al., 2009; van Damme et al.,
56 2009). However, the molecular and physiological mechanism of how chloroplast
57 weaponry is launched against invading pathogens is unclear.

58 Here we show that to counteract host cell invasion by the Irish potato famine pathogen

59 *P. infestans*, chloroplasts navigate to pathogen penetration sites. Photo-relocation
60 component chloroplast unusual positioning 1 (CHUP1) (Oikawa et al., 2008, 2003)
61 mediates chloroplast accumulation around the haustorium by facilitating anchoring to the
62 host-derived perimicrobial membrane interface. Moreover, stromule development
63 increases upon *P. infestans* infection, in a CHUP1 dependent manner. Stromules
64 embrace haustoria and mediate physical interactions between chloroplasts, forming
65 dynamic clusters around the pathogen interface. Notably, infection-triggered stromule
66 development relies on surface immune signalling, whereas the pathogen subverts this
67 remotely by switching off surface immune pulses. These results implicate chloroplast
68 photo-relocation machinery in plant focal immune responses and demonstrate that
69 chloroplasts play a direct role in antagonizing pathogen invasion.

70 **Results & Discussion:**

71 To gain insights into defence-related chloroplast functions, we investigated chloroplast
72 dynamics during *P. infestans* infection of the solanaceous model plant *Nicotiana*
73 *benthamiana*. Confocal microscopy of infected leaf epidermal cells stably expressing
74 GFP in chloroplast stroma (CpGFP hereafter) revealed that chloroplasts accumulate at
75 58% of haustoria ($n = 299$ haustoria) (Fig. 1A-C). Notably, chloroplasts are mainly
76 positioned around infection sites, sieging haustoria in a highly dynamic fashion (Fig. 1C,
77 1E and Movie S1-3). Furthermore, compared to non-infected controls, we recorded a 5-
78 fold increase in stromule formation in infected CpGFP cells (Fig. 1A-B, 1D). Notably,
79 chloroplasts seized haustoria, tightly embracing the EHM through stromules that extend
80 and coil around the pathogen (Fig. 1A, 1C, Movie S3). Expression of the EHM marker
81 protein RFP:REM1.3 (Bozkurt et al., 2014) in infected CpGFP plants, allowed us to
82 collect further evidence that chloroplasts intimately associate with the EHM (Fig. S1,
83 Movie S4). Remarkably, time lapse-microscopy showed that chloroplasts plunge towards
84 haustoria and embrace the EHM following haustorial penetration (Fig. 1E, Movie S5, Fig.
85 S2), suggesting that chloroplasts may participate in focal immunity.

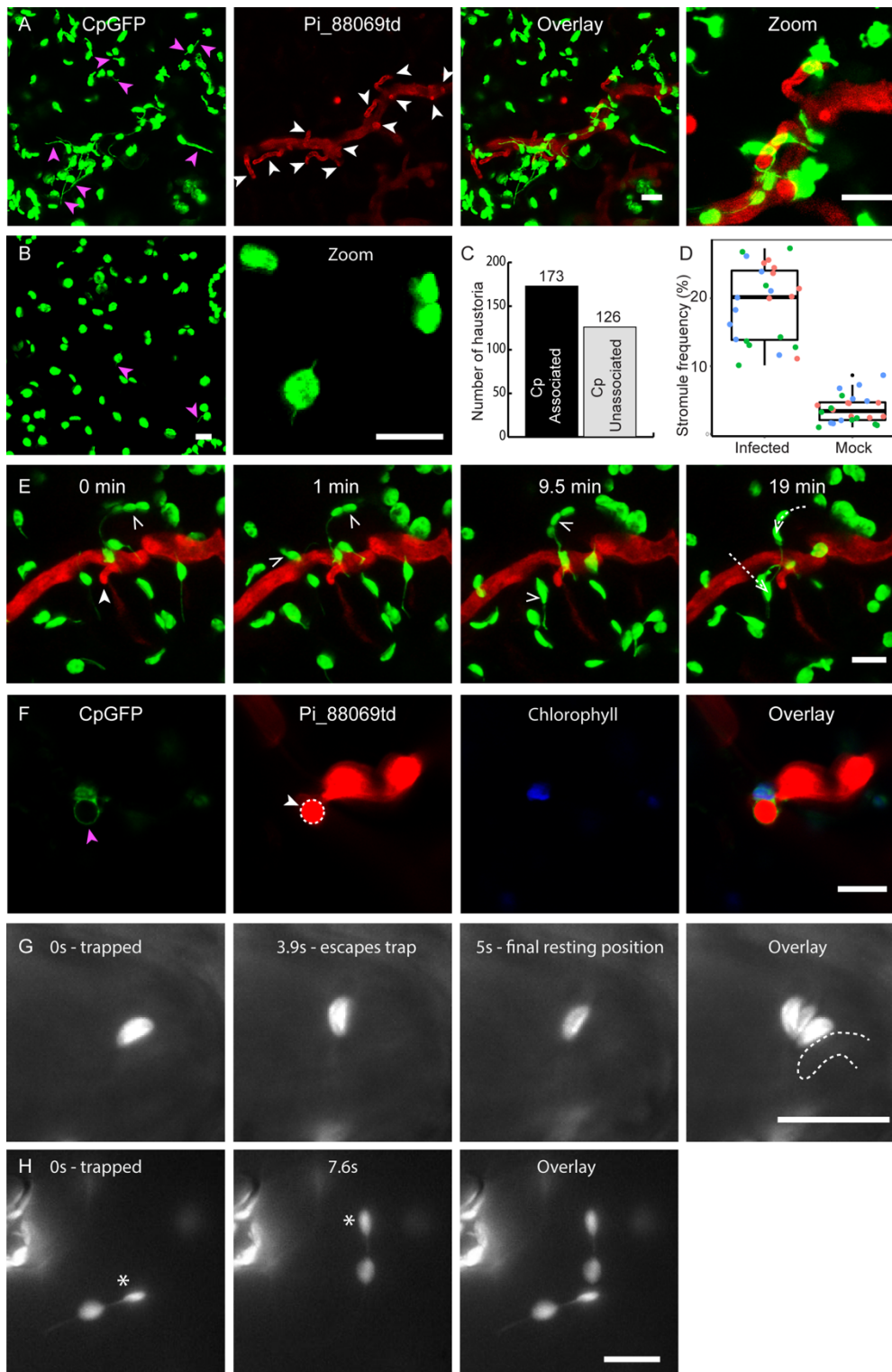
86 To determine the extent to which chloroplasts physically associate with the EHM, we
87 next employed optical tweezers in combination with Total Internal Fluorescence
88 Microscopy (TIRF) in infected CpGFP plants. Using optical tweezers, we successfully
89 trapped and moved 17% of chloroplasts ($n = 29$) in non-haustoriated cells, a distance
90 greater than the 10 μm threshold. In comparison, we were unable to trap and move any
91 chloroplasts (0%, $n = 18$) neighbouring haustoria past the threshold, indicating a strong
92 association between the chloroplasts and the EHM. Consistent with this, we recorded a
93 few instances where these chloroplasts were initially pulled away from the EHM, but
94 before they passed the distance threshold they escaped the trap and sprang back

95 towards their former position (22%, $n = 18$) (Fig. 1G, Movie S6). Taken together, these
96 results demonstrate that chloroplasts mobilize towards haustoria and tightly embrace the
97 EHM through induction of stromules, possibly to increase the surface area of interaction,
98 in a manner similar to chloroplast-nucleus communication upon activation of antiviral
99 immunity (Kumar et al., 2018).

100 Remarkably, upon pathogen infection, we noted that chloroplasts frequently formed
101 dynamic clusters via stromules, occasionally bridging multiple haustoria (Fig. 1A, Fig.
102 S3, Movie S1, S7, S8). Optical trapping of chloroplasts in pathogen-challenged tissue
103 illustrated co-migration of chloroplast pairs interconnected by a stromule like extension
104 (Fig. 1H, and Movie S9), indicating that chloroplasts can be physically linked. Both
105 observations raise the possibility that chloroplasts might coordinate their defence-related
106 tasks cooperatively to respond to pathogen attack. However whether plastids can fuse to
107 form a continuous stromal compartment that enables macromolecule exchange thorough
108 stromules is debated (Hanson and Hines, 2017; Schattat et al., 2014).

109 Intriguingly, although rarely observed, we captured two time-lapse image series, which
110 show collapse of the haustoria during chloroplast steering (Fig. S4, Movie S10, S11).
111 This prompted the idea that in addition to their biochemical arsenal (de Torres Zabala et
112 al., 2015; Serrano et al., 2016; Trotta et al., 2014), chloroplasts plausibly harness
113 mechanical means to oppose pathogen penetration. Supporting this view, we recorded
114 time-lapse series of chloroplast clusters adjacent to haustoria which moved
115 simultaneously in the same direction (Movie S12, S13).

116



117

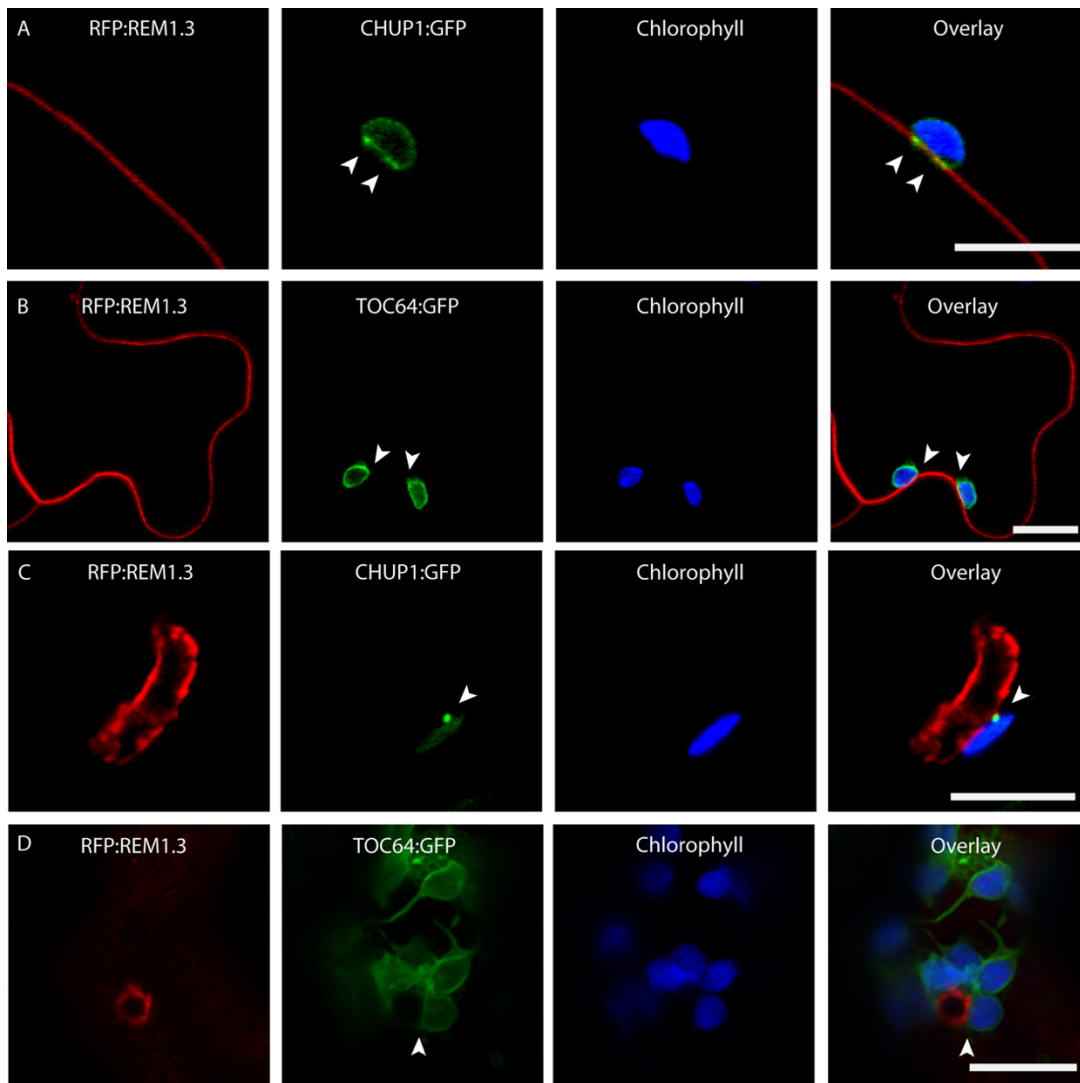
118 **Fig. 1. Chloroplasts move towards haustoria and associate with the EHM via**
119 **stromule induction.** (A-B, E-F) Maximum projection confocal micrographs of *N.*
120 *benthamiana* plants expressing GFP in chloroplast stroma (CpGFP). (A) Stromule

121 induction and chloroplast accumulation around haustoria with *P. infestans* strain 88069td
122 compared to (B) Mock inoculated cells. (C) Number of 88069td haustoria associated with
123 one or more chloroplast. (D) Scatter box-plot shows increased stromule induction ($p <$
124 0.01) in infected ($n = 24$ images quantified) vs uninfected ($n = 24$ images quantified)
125 tissue. (E) Maximum intensity projection time-lapse series showing movement of tracked
126 chloroplasts (open arrowheads) towards haustorium. Dashed line indicates approximate
127 path travelled. (F) Single plane image showing stromule (purple arrowhead) wrapped
128 around haustorium (white arrowhead). (G-H) GFP channel in grayscale from TIRF
129 microscope. Time-lapse showing laser capture of haustorium associated chloroplast in
130 CpGFP plant where automated the trapping routine, traps and attempts to move
131 chloroplast $10 \mu\text{m}$. (G) Chloroplast which escapes laser trap, reaching the furthest
132 possible point from haustorium (3.9 s) before springing back (5.0 s). Dotted line shows
133 outline of haustorium marked by RFP:REM1.3. (H) Trapped chloroplast (asterisk) linked
134 by stromule to another chloroplast. When the trapped chloroplast moves, the linked
135 chloroplast co-migrates. Scale bars: $10 \mu\text{m}$.

136

137 To elucidate the role of chloroplast positioning in plant cell invasion of *P. infestans*, we
138 investigated whether a relationship exists between light and pathogen-induced
139 chloroplast movements. We particularly focused on chloroplast unusual positioning 1
140 (CHUP1), a protein that regulates chloroplast photo-relocation, movement and anchoring
141 to the plasma membrane (Oikawa et al., 2008, 2003). Similar to a GFP fused chloroplast
142 envelope marker protein, translocon at the outer membrane of chloroplasts 64
143 (TOC64:GFP), CHUP1:GFP labelled the chloroplast outer envelope (Fig 2A & B).
144 However, CHUP1:GFP displayed an unusually increased fluorescence intensity at foci
145 across the chloroplast-plasma membrane interface (Fig. 2A). Notably, in haustoriated
146 cells, CHUP1:GFP accumulated at chloroplast-EHM contact sites (Fig. 2C, Fig. S5),

147 whereas TOC64:GFP uniformly labelled the chloroplast envelope without producing any
148 fluorescent foci adjacent to the EHM (Fig. 2D). The discrete punctate localisation of
149 CHUP1:GFP at the EHM contact sites suggested that CHUP1 could mediate anchoring
150 of chloroplasts to the EHM which typically lacks plasma membrane proteins (Bozkurt et
151 al., 2015, 2014; Whisson et al., 2016). These results indicate that CHUP1, a core
152 component of the chloroplast photo-relocation machinery, might be co-opted for
153 chloroplast recruitment to the pathogen interface.



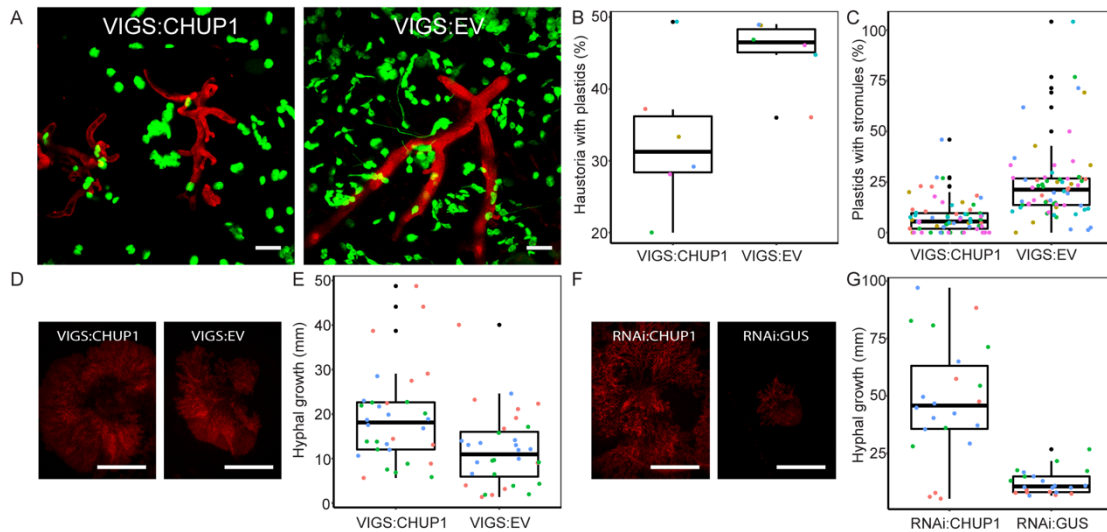
154

155 **Fig. 2. CHUP1 localizes to the chloroplast outer envelope and accumulates at**
156 **contact points between plastids and the plasma membrane or EHM.** Single-plane
157 confocal microscope images of wild-type *N. benthamiana* transiently co-expressing
158 plasma membrane and EHM marker RFP:REM1.3 with CHUP1:GFP (A & C) or
159 TOC64:GFP (B & D). (A) CHUP1:GFP labels chloroplast outer membrane and
160 accumulates at contact points (white arrowheads) with the plasma membrane. (B)
161 TOC64:GFP distributes uniformly across the chloroplast outer membrane. (C)
162 CHUP1:GFP accumulates at *P. infestans* EHM contact points. (D) TOC64:GFP displays
163 a uniform distribution when in contact with the EHM. Scale bars: 10 μ m.

164 We next set out to determine whether CHUP1 is required for pathogen directed
165 chloroplast movement and EHM docking. Remarkably, downregulation of *CHUP1*
166 expression through virus-induced gene silencing (VIGS) in infected CpGFP plants,
167 significantly reduced the number of haustoria that associate with chloroplasts (33%, $n =$
168 544 haustoria) compared to the silencing control (45%, $n = 471$ haustoria) (Fig. 3A-B,
169 Fig. S6). We obtained similar results following RNA interference (RNAi) mediated
170 knockdown of *CHUP1* in both wild-type *N. benthamiana* and CpGFP plants (Fig. S7).
171 These results indicate that CHUP1 facilitates chloroplast recruitment to the pathogen
172 interface, where it accumulates, likely through mediating chloroplast anchoring to the
173 EHM (Fig. 2C). In addition, VIGS mediated knock down of *CHUP1* reduces stromule
174 induction (8% chloroplasts with stromule(s), $n = 68$ images quantified) compared to
175 control silencing (2% chloroplasts with stromule(s), $n = 68$ images quantified),
176 suggesting that CHUP1 is required for pathogen induced stromule development (Fig.
177 3C). Likewise, in infected CpGFP plants, transient RNAi of CHUP1 led to a 2-fold
178 decrease in stromule induction (18% chloroplasts with stromule(s), $n = 11$ images
179 quantified) compared to the GUS-silencing control (39% chloroplasts with stromule(s), n
180 = 10 images quantified) (Fig. S7). Collectively, these results demonstrate that CHUP1 is
181 essential for both pathogen-directed chloroplast mobility and infection-triggered
182 stromules formation which is implicated in antimicrobial immunity (Caplan et al., 2015),
183 pointing to a positive role of CHUP1 in plant immunity.

184 We next tested the hypothesis that the process of chloroplast positioning and anchoring
185 to the pathogen interface enhances disease resistance. VIGS of *CHUP1* led to
186 considerably higher levels of *P. infestans* hyphal growth compared to the silencing
187 control (Fig. 3D-E). We repeated these infection assays following RNAi-mediated
188 silencing of *CHUP1*. Consistently, RNAi of *CHUP1* substantially enhanced filamentous

189 growth of *P. infestans* compared to RNAi-GUS control (Fig. 3F-G). Taken together,
190 these results indicate that CHUP1 contributes to plant focal immunity, possibly through
191 coordinating chloroplast navigation to the EHM. However, since CHUP1 is also essential
192 for induction of stromules that intimately associate with the EHM, we infer that processes
193 such as chloroplast steering and docking to the pathogen interface as well as formation
194 of stromules are a series of interconnected events to counteract microbial invasion.

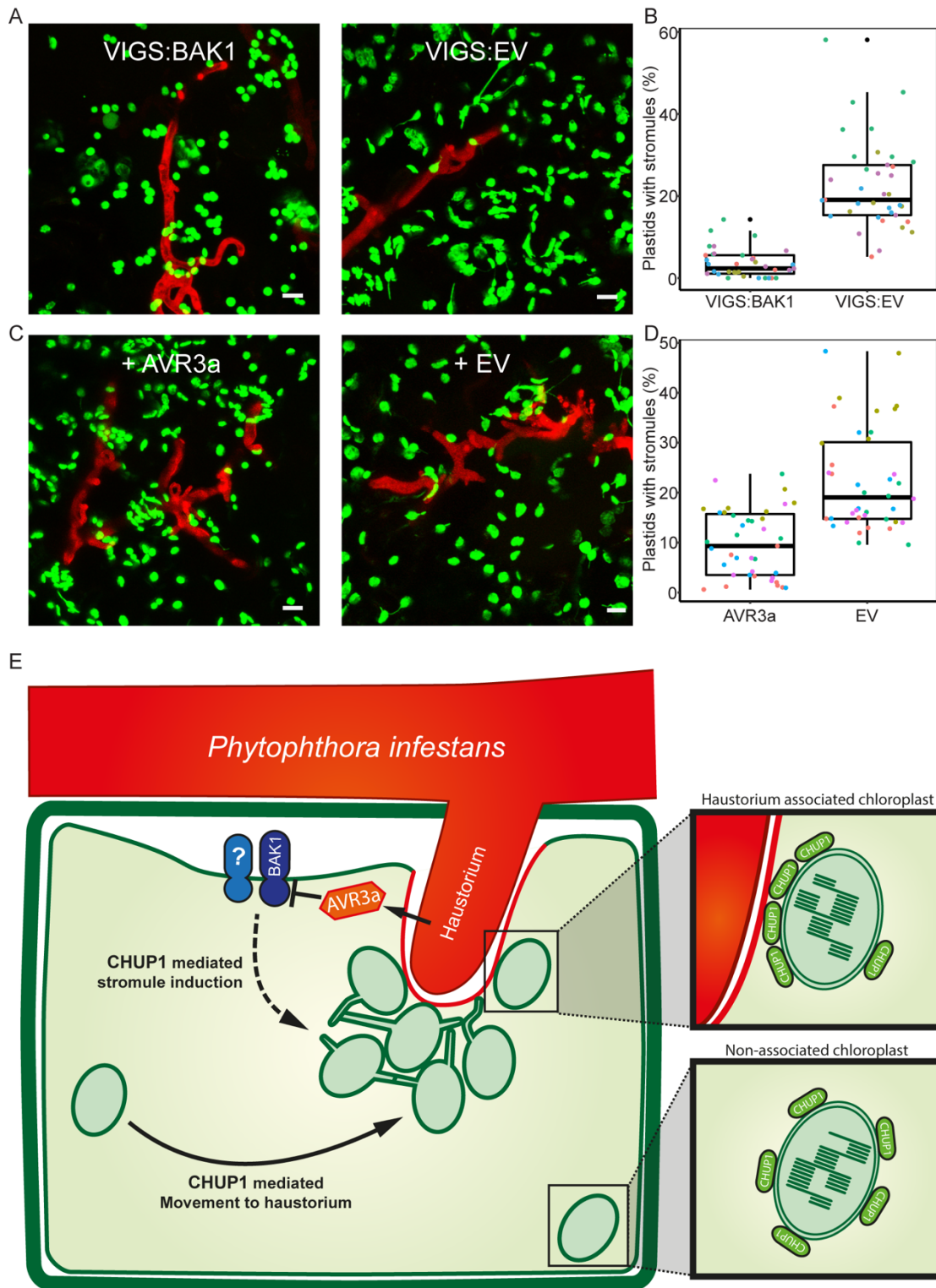


195

196 **Fig. 3. CHUP1 silencing decreases immunity to *P. infestans*, perihyphal**
197 **chloroplast accumulation and stromule induction (A)** Maximum-projection confocal
198 micrographs of CpGFP leaf epidermal cells, where *CHUP1* is systemically silenced
199 (VIGS), and infected with 88069td. VIGS-empty vector (EV) included as control. Scale
200 bars: 10 μm. (B) Scatter-boxplot shows reduced percentage of haustoria associated with
201 plastid(s) ($p < 0.01$) in VIGS-CHUP1 plants (33% of $n = 544$ haustoria), compared to
202 VIGS-EV plants (45% of $n = 471$ haustoria). (C) Scatter-boxplot depicts reduction in
203 stromule induction ($p < 0.01$) in VIGS-CHUP1 plants (8%, $n = 68$ images quantified),
204 compared to VIGS-EV plants (24%, $n = 68$ images quantified). (D-G) Silencing of
205 *CHUP1* by VIGS or transient RNAi, followed by 88069td inoculation shows CHUP1
206 contributes to resistance. Hyphal growth measured using fluorescence
207 stereomicroscope at 4 dpi for VIGS (D) and 6 dpi for transient RNAi (F). Scale bars: 10
208 mm. (E & G) Scatter-boxplots show mean area of hyphal growth for inoculations on
209 VIGS leaves, $n = 32$ leaves per treatment ($p < 0.01$) (E), and transient RNAi silenced
210 leaves, $n = 22$ leaves for each experiment ($p < 0.01$).

211 Finally, to gain further insights into the interplay between chloroplasts and haustoria, we
212 investigated the means of pathogen induced stromule formation. Stromule development
213 was previously reported to be induced upon cytoplasmic recognition of bacterial
214 effectors or viral particles by NLR (nucleotide-binding domain and leucine-rich repeat-
215 containing) receptors (Caplan et al., 2015; Erickson et al., 2018; Krenz et al., 2012).
216 However, because *P. infestans* establishes a compatible interaction with *N.*
217 *benthamiana* without activating NLR triggered immunity, we reasoned that stromule
218 development could be stimulated through surface immune recognition (Caplan et al.,
219 2015). Thus, we monitored stromule formation upon silencing of *BAK1* (Fig. S8), a
220 surface localized co-receptor that mediates immune signalling through various PRRs
221 (Chaparro-Garcia et al., 2011; Perraki et al., 2018; Smakowska-Luzan et al., 2018).
222 Remarkably, in five independent experiments, we noticed a substantial decrease in
223 infection triggered stromule induction following *BAK1* silencing (4%, $n = 37$ images
224 quantified) in relation to control silencing (23%, $n = 37$ images quantified) (Fig. 4A-B).

225 We then tested whether AVR3a, a host-translocated effector of *P. infestans* that
226 suppresses BAK1-mediated immune signalling (Bos et al., 2010; Chaparro-Garcia et al.,
227 2011), can perturb pathogen induced stromule development. Notably, following
228 heterologous expression of AVR3a (Fig. S9), infection-triggered stromule formation
229 decreased by more than two-fold (Fig. 4C-D). These results demonstrate that stromules
230 are induced during *P. infestans* host colonization through surface immune signalling,
231 whereas the pathogen deploys effectors to counteract this process, further supporting
232 the defence-related role of stromules. Since stromule induction is CHUP1-dependent,
233 we conclude that CHUP1 contributes to immunity through mediating chloroplast
234 navigation and chloroplast interaction via diverse signalling stimuli, which are
235 coordinated to prevent host cell invasion of filamentous pathogens (Fig. 4E, model).



236

237 **Fig. 4: *P. infestans* induces stromules through surface recognition. (A-B)**

238 Systemically silencing *BAK1* (VIGS-BAK1) reduces stromule induction during infection,

239 compared with EV control. (A) Maximum projection confocal microscopy images of
240 CpGFP leaves silenced with VIGS-BAK1 or VIGS-EV, infected with 88069td. (B) Scatter-
241 boxplot depicts reduction in stromule induction ($p < 0.01$) in VIGS-BAK1 plants (4%, $n =$
242 37 images quantified), compared to VIGS-EV plants (23%, $n = 37$ images quantified).
243 (C) Overexpression of *P. infestans* effector AVR3a reduces stromule induction during
244 infection with 88069td in CpGFP. (D) Scatter-boxplot shows transient AVR3a expression
245 reduces stromule induction (9%, $n = 39$ images quantified) compared to EV expression
246 (22%, $n = 40$ images quantified) ($p < 0.01$). (E) Model: Surface recognition of *P. infestans*
247 leads to CHUP1-dependent stromule induction. CHUP1 mediates chloroplast movement
248 to siege haustoria and develop inter-chloroplast clustering at the penetration site.

249 Our results demonstrate that chloroplasts navigate to the pathogen interface and
250 establish secure membrane contacts with the EHM to contribute to focal immunity (Fig.
251 1, Fig. S1-2, Movie S5). These processes are dependent on CHUP1, a key component
252 of blue-light-induced chloroplast movement and plasma membrane attachment
253 (Kasahara et al., 2002; Oikawa et al., 2008), indicating that chloroplast photo-relocation
254 machinery is co-opted for antimicrobial immunity. Remarkably, CHUP1 accumulates at
255 the chloroplast-EHM interface (Fig. 2C, Fig. S4), possibly to enable stronger membrane
256 attachment, as has been shown in plasma membrane docking of chloroplasts (Kadota et
257 al., 2009).

258 We show that surface immune activation induces stromule development into a large,
259 intricate web of chloroplasts (Fig. 1A, 1H, Fig. S3, Movie S1, S3, S7-9). These are
260 reminiscent of mitochondrial networks with poorly understood functions (Hoitzing et al.,
261 2015). Intricate chloroplast clusters could boost coordination of their defence-related
262 functions by, for instance, mediating focal deployment of chloroplast weaponry at the
263 pathogen interface. In addition, a speculative hypothesis is that chloroplast clusters
264 could also generate mechanical forces to repulse infection structures that invade the
265 plant cells, as has been suggested by our live cell imaging (Fig. S10-13). However, we
266 show that adapted pathogens can remotely counteract stromule development by
267 deploying effectors that shut down surface immune signalling (Fig. 4B). Conceivably, this
268 would dismantle chloroplast stromules and reduce the surface area of the chloroplasts in
269 contact with the EHM. These findings further support the notion that stromules are
270 induced to contribute to pathogen defence (Caplan et al., 2015; Erickson et al., 2018).
271 Our findings implicate chloroplasts in polarized immune responses of plants against
272 filamentous pathogens and point to more complex, direct defence-related functions for
273 chloroplasts.

274 **Materials and Methods**

275 Biological Material

276 *Nicotiana benthamiana* plants grown in a growth chamber at 25°C under high light
277 intensity (16-h-day/8-h-dark photoperiod) were used for all experiments. Transplastomic
278 GFP-expressing *Nicotiana benthamiana* plants, accumulating GFP in the chloroplast
279 stroma (Stegemann et al., 2012) were maintained in the same conditions. *Phytophthora*
280 *infestans* isolate 88069 (WT) (Van West et al., 1998) and 88069td (TD) (Whisson et al.,
281 2007), a transgenic strain expressing the red fluorescent marker tandem dimer RFP
282 (tdTomato), were used. Both isolates were cultured on plates with rye sucrose agar
283 (RSA) for 12-16 days at 18°C in the dark, as described elsewhere (Song et al., 2009)
284 prior to use for infection of *N. benthamiana*.

285

286 Molecular Cloning and plasmid constructs

287 The following constructs used in this study were previously published as follows:
288 RFP:REM1.3 (Bozkurt et al., 2014); TOC64:GFP (Breuers et al., 2012); AVR3a cloned in
289 pICSL86977 was provided by TSLSynBio. CHUP1:GFP construct was cloned using
290 Gibson Assembly Protocol (Gibson et al., 2009). Briefly, CHUP1:GFP was generated by
291 amplifying two PCR products (Phusion DNA polymerase, Thermo Scientific) from *N.*
292 *benthamiana* cDNA, amplifying *CHUP1-a* (herein *CHUP1*) using two different primer
293 pairs (CHUP1-A F; GA_CHUP1_R1; GA_CHUP1B_F2; GA_CHUP1B_R2). The PCR
294 products were assembled and cloned into the destination vector pK7FWG2,0 (GFP) by
295 Gibson assembly. The purified vector was transformed into *A. tumefaciens* competent
296 cells. RNAi-silencing constructs for CHUP1 were cloned using the Gateway Cloning
297 Technology. RNAi-CHUP1 construct was generated to target a region in the middle of

298 the gene (942-1200bp)(Helliwell and Waterhouse, 2003). The selected sequence was
299 synthesized and cloned into pK7GWIWG2(II) vector(Karimi et al., 2002). VIGS vector
300 pTRV2-CHUP1 was assembled by amplifying a 500bp region of *Chup1* (the same region
301 targeted as previously(Caplan et al., 2015)) from *N. benthamiana* cDNA using primers
302 VIGS_CHUP1_F and VIGS_CHUP1_R2. The amplified fragment was then cloned into a
303 Gateway compatible pTRV2 vector using Gateway Technology (Invitrogen). Silencing
304 construct TRV2-BAK1 was kindly provided by The Sainsbury Lab(Chaparro-Garcia et
305 al., 2011).

306

307 Transient gene-expression assays in *N. benthamiana*

308 *Agrobacterium tumefaciens* GV3101 strain(Hellens et al., 2000) carrying T-DNA
309 constructs was used to mediate transient gene expression (Agroinfiltration) into 3-4-
310 week-old *N. benthamiana* leaves, as previously described(Bozkurt et al., 2014, 2011).
311 Briefly, overnight cultures of transformed *A. tumefaciens* were washed and harvested
312 with 1500 µl autoclaved dH₂O by centrifugation at 1500g twice and resuspended in
313 agroinfiltration buffer (10 mM 2-(*N*-morpholino-ethanesulfonic acid hydrate (MES
314 hydrate), 10 mM MgCl₂, pH 5.7). For the transient co-expression assays, each *A.*
315 *tumefaciens* construct was mixed in agroinfiltration buffer to achieve a final OD₆₀₀ of 0.2
316 or 0.3 for each *A. tumefaciens*, depending on the experiment. *P. infestans* inoculations
317 were performed 4 to 24h after infiltrations.

318

319 Virus induced gene silencing (VIGS)

320 *Agrobacterium* was prepared as above carrying TRV1 and the appropriate TRV2
321 construct and mixed to a final OD₆₀₀ of 0.4 or 0.2 respectively, in agroinfiltration buffer

322 supplemented with 100 μ M acetosyringone (Sigma) and left in the dark for 2 h prior to
323 infiltration to stimulate virulence. 14-day old *N. benthamiana* seedlings were infiltrated in
324 both cotyledons and any true leaves that had emerged. *N. benthamiana* plants were
325 infiltrated with TRV1 and TRV2-CHUP1 for CHUP1-silencing and TRV1 and TRV2-EV
326 for the empty vector control. TRV2 containing the *N. benthamiana* sulfur (Su) gene
327 fragment (TRV2-NbSU) was used as a positive control to indicate viral spread. Plants
328 were left to grow under standard conditions until experiments could be carried out four
329 weeks later.

330

331 Infection assays

332 Infection assays to assess the effect of *CHUP1* silencing on *P. infestans* colonization
333 were performed as follow: for RNAi experiments, *A. tumefaciens* containing RNAi-
334 CHUP1 or RNAi-GUS (OD₆₀₀ = 0.3) constructs were infiltrated for transient expression
335 side by side on either halves of independent *N. benthamiana* leaves, 24h prior to
336 infection. For VIGS experiments, 3 weeks after silencing was initiated leaves were
337 detached for infection from VIGS-CHUP1 and VIGS-empty vector plants. Zoospores
338 were harvested from sporangia by addition of cold distilled water and collected after 2h
339 of incubation at 4°C, adjusting dilution to 50,000 spores/ml. Infection assays were
340 performed by the addition of 10 μ l of zoospore droplets to the base, middle and tip of the
341 abaxial side of each leaf, 3 on each side, as described previously(Saunders et al., 2012;
342 Song et al., 2009). The infected leaves were maintained in plastic boxes on damp paper
343 towels at 18°C under 16-h- day/8-h-night conditions, and inoculated with *P. infestans*
344 88069td. Images of hyphal growth were captured on a Leica DFC300 FX fluorescent
345 microscope (Leica Microsystems, Germany) using the DSR UV filter at the timepoints
346 indicated in the Fig. legends. Images were processed in ImageJ (2.0) and quantification

347 of hyphal growth was performed by measuring the diameter in mm² of hyphal growth of
348 each infected spot.

349

350 RT-PCR assay

351 60 mg of leaf tissue was excised from 4-week-old *N. benthamiana* leaves (RNAi
352 experiment, 6 days after silencing), and 5-week old leaves (VIGS experiments) and
353 frozen in liquid N₂. RNA was extracted from the leaf tissue using the Plant RNA Isolation
354 Mini Kit Protocol (Agilent Technologies). RNA quality and concentration was measured
355 using a NanoDropTM Lite Spectrophotometer (Thermo Scientific). cDNA was
356 synthesized using as a template 2 µg of RNA following the SuperScript II RT protocol
357 (Invitrogen). To amplify the cDNA, a standard PCR (RT-PCR) was then performed using
358 DreamTaq DNA polymerase (5 u/µl) (Thermo Scientific). RNAi-CHUP1 construct effect
359 on *CHUP1* downregulation was evaluated by RT-PCR using primers CHP1_RT_F1 and
360 BD-CHUP1-REV. VIGS-CHUP1 silencing was confirmed with CHUP1a_RT_F &
361 CHUP1a_RT_R, which specifically amplifies *CHUP1a*, and CHUP1b_RT_F &
362 CHUP1b_RT_R, which specifically amplifies *CHUP1b*. VIGS-BAK1 silencing was
363 confirmed as previously described(Chaparro-Garcia et al., 2011).

364

365 Confocal microscopy

366 All microscopy analyses were performed on live *N. benthamiana* epidermal cells 2-6
367 days post agroinfiltrations and infections. Leaf discs were excised and imaged on a
368 Leica SP5 resonant inverted confocal microscope (Leica Microsystems) using 63X
369 1.2NA Plan-Apochromat water immersion objective. Specific excitation wavelengths and
370 filters for emission spectra were set as described previously(Koh et al., 2005). The

371 Argon laser excitation was set to 488 nm and the Helium-Neon laser to 543 nm and their
372 fluorescent emissions detected at 495–550 and 570–620 nm to visualize GFP and RFP
373 fluorescence, respectively. To avoid bleed-through from different fluorophores, images
374 were acquired using sequential scanning and Maximum Intensity Projections were
375 created from the Z-stacks. 3D images and movies were generated with confocal files in
376 12-bit TIFF format imported into NIS-Elements (Version 4.50, Nikon Instruments, UK)
377 and processed with Advanced Denoising. Movies were made using the Volume View
378 and Movie Maker modules

379

380 Optical trapping setup

381 Optical trap for chloroplast/stromule capture was setup as described by Sparkes et al
382 2017, Chapter 13(Hawes, 2018, chap. 13). An optical trap with a two-channel TIRF
383 microscope (TIRF-M) was combined with a Nikon Ti-U inverted microscope. Optical
384 trapping was performed using a near infrared trapping laser at 1070 nm using a Nikon
385 100x, oil immersion, NA 1.49 TIRF objective lens. For GFP and RFP chromophores
386 fused to the proteins of interest were excited using 488 and 561 nm laser diode,
387 respectively. Their Fluorescent emissions were detected using two electron multiplying
388 charge-coupled device (EMCCD, iXon, Andor) cameras. The sample (~5 mm² leaf
389 tissue) was mounted on a computer-controlled variable speed (Märzhäuser) stepper
390 motor stage. The associated computer-controlled hardware was interfaced using
391 National Instruments LabVIEW which provides full automation for each trapping routine.
392 The power of the optical trap laser transmission was set to 40.7 mW. The TIRF image
393 was recorded from 0 s, the trap was turned on at 1 s, the translation stage movement of
394 10 µm at 2 µm/s begins at 5 s and ends at 10 s, the trap was deactivated at 11 s, and
395 the image recording stops at 22 s (relating to 11 s recovery periods).

396 Bioinformatic and statistical analysis

397 In order to identify putative orthologs of *Arabidopsis thaliana* for CHUP1 in *N.*
398 *benthamiana* genome, a TBLASTN search using the protein sequence of *CHUP1* from
399 *A. thaliana* against the *N. benthamiana* cDNA was accomplished in Solgenomics. Two
400 orthologs (*CHUP1-a* and *CHUP1-b*) of *Arabidopsis CHUP1* gene were identified in *N.*
401 *benthamiana* genome. Chloroplast quantification was done automatically using a
402 MATLAB script. Stromules were manually counted using a semi-automated MATLAB
403 script. Percentage of chloroplasts with stromules were calculated by dividing the number
404 of chloroplasts one (or more) stromule(s) by the total number of chloroplasts.
405 Quantification of hyphal growth was accomplished by measuring the diameter of the
406 lesion on each inoculated spot using Fiji image-processing software. R package was
407 used to visualize the values from three to four independent biological replicates by
408 generating scatter plots. Statistical significance of the differences observed were
409 assessed by t test when found to be normal by sharpiro test. If data was found to be
410 non-normally distributed Wilcox statistical test was implemented by R package.

411

412 Chloroplast automated counting algorithm through image processing

413 The image processing algorithms were used to calculate the gradient of the image to
414 identify the boundaries of the puncta. Enclosed regions formed by the boundaries were
415 algorithmically identified and counted. This procedure was done for each individual
416 channel green (in chloroplast stroma) and blue (Chloroplast Auto-fluorescence). The
417 chloroplast (GFP channel) containing stromule were counted in a semi-automated
418 fashion.

419 **Acknowledgements:** We thank Dr. Alex Jones (Warwick) for initiating collaboration with
420 IS, Dr. Sebastian Schornack (SLCU) for initiating collaboration with MS, Prof. Peter
421 Nixon (Imperial) for providing CP-GFP plant seeds. **Funding:** Bozkurt lab funded by
422 BBSRC (BB/M002462/1). The Facility for Imaging by Light Microscopy (FILM) at Imperial
423 College London is part-supported by funding from the Wellcome Trust (grant
424 104931/Z/14/Z) and BBSRC (grant BB/L015129/1). **Author contributions:**
425 Conceptualization: CD, ZS, MES, IS, MS, TOB; Data curation: AT, CD, PP, ZS, DCAG,
426 BCB, LHY, IS, TOB; Formal analysis: AT, CD, PP, ZS, BCB, IS, TOB; Funding
427 acquisition: TOB; Investigation: AT, CD, PP, ZS, MES, LHY, AYL, VK, BCB, TOB;
428 Methodology: AT, CD, ZS, DCAG, ADW, SWB, BCB, IS, MS, TOB; Project
429 Administration: CD, TOB; Resources: AT, CD, AYL, VK, IP, IS, TOB; Software: IP;
430 Supervision: AT, CD, PP, MES, BCB, IS, TOB; Validation: AT, CD, PP, ZS, MES, IS,
431 MS; Visualisation: CD, ZS, TOB; Writing – original draft: CD, ZS, TOB; Writing – review
432 & editing: AT, CD, PP, ZS, MES, LHY, DCAG, AYL, ADW, SWB, MS, IS, TOB.
433 **Competing interests:** Authors declare no competing interests. **Data and materials**
434 **availability:** All data is available in the main text, the supplementary materials or other
435 raw data is available upon request. We are happy to provide all materials used here
436 upon request.

437 **References:**

- 438 Belhaj K, Lin B, Mauch F. 2009. The chloroplast protein RPH1 plays a role in the
439 immune response of Arabidopsis to *Phytophthora brassicae*. *Plant J* **58**:287–298.
440 doi:10.1111/j.1365-313X.2008.03779.x
- 441 Bos JIB, Armstrong MR, Gilroy EM, Boevink PC, Hein I, Taylor RM, Zhendong T,
442 Engelhardt S, Vetukuri RR, Harrower B, Dixelius C, Bryan G, Sadanandom A,
443 Whisson SC, Kamoun S, Birch PRJ. 2010. *Phytophthora infestans* effector AVR3a
444 is essential for virulence and manipulates plant immunity by stabilizing host E3
445 ligase CMPG1. *Proc Natl Acad Sci* **107**:9909–9914. doi:10.1073/pnas.0914408107
- 446 Bozkurt TO, Belhaj K, Dagdas YF, Chaparro-Garcia A, Wu C-H, Cano LM, Kamoun S.
447 2015. Rerouting of plant late endocytic trafficking toward a pathogen interface.
448 *Traffic* **16**:204–26. doi:10.1111/tra.12245
- 449 Bozkurt TO, Richardson A, Dagdas YF, Mongrand S, Kamoun S, Raffaele S. 2014. The
450 Plant Membrane-Associated REMORIN1.3 Accumulates in Discrete Perihaustorial
451 Domains and Enhances Susceptibility to *Phytophthora infestans*. *Plant Physiol*
452 **165**:1005–1018. doi:10.1104/pp.114.235804
- 453 Bozkurt TO, Schornack S, Win J, Shindo T, Ilyas M, Oliva R, Cano LM, Jones AME,
454 Huitema E, van der Hoorn R a L, Kamoun S. 2011. *Phytophthora infestans* effector
455 AVRblb2 prevents secretion of a plant immune protease at the haustorial interface.
456 *Proc Natl Acad Sci U S A* **108**:20832–7. doi:10.1073/pnas.1112708109
- 457 Breuers FKH, Bräutigam A, Geimer S, Welzel UY, Stefano G, Renna L, Brandizzi F,
458 Weber APM. 2012. Dynamic Remodeling of the Plastid Envelope Membranes – A
459 Tool for Chloroplast Envelope in vivo Localizations. *Front Plant Sci* **3**:1–10.
460 doi:10.3389/fpls.2012.00007
- 461 Brodersen P, Achard, Lali Sakvarelidze Rasmussen MB, Dunoyer P, Yamamoto YY,
462 Sieburth L, Voinnet O. 2008. Widespread Translational Inhibition by Plant miRNAs

- 463 and siRNAs. *Science* (80-) **320**:1185–1190.
- 464 Caplan JL, Kumar AS, Park E, Padmanabhan MS, Hoban K, Modla S, Czymmek K,
465 Dinesh-Kumar SP. 2015. Chloroplast Stromules Function during Innate Immunity.
466 *Dev Cell* **34**:45–57. doi:10.1016/j.devcel.2015.05.011
- 467 Chaparro-Garcia A, Wilkinson RC, Gimenez-Ibanez S, Findlay K, Coffey MD, Zipfel C,
468 Rathjen JP, Kamoun S, Schornack S. 2011. The receptor-like kinase serk3/bak1 is
469 required for basal resistance against the late blight pathogen *Phytophthora*
470 *infestans* in *Nicotiana benthamiana*. *PLoS One* **6**.
471 doi:10.1371/journal.pone.0016608
- 472 Dagdas YF, Pandey P, Tumtas Y, Sanguankiattichai N, Belhaj K, Duggan C, Leary AY,
473 Segretin ME, Contreras MP, Savage Z, Khandare VS, Kamoun S, Bozkurt TO.
474 2018. Host autophagy machinery is diverted to the pathogen interface to mediate
475 focal defense responses against the Irish potato famine pathogen. *Elife* 1–15.
476 doi:10.7554/eLife.37476
- 477 de Torres Zabala M, Littlejohn G, Jayaraman S, Studholme D, Bailey T, Lawson T,
478 Tillich M, Licht D, Bölter B, Delfino L, Truman W, Mansfield J, Smirnov N, Grant M.
479 2015. Chloroplasts play a central role in plant defence and are targeted by
480 pathogen effectors. *Nat Plants* **1**:15074. doi:10.1038/nplants.2015.74
- 481 Erickson JL, Adlung N, Lampe C, Bonas U, Schattat MH. 2018. The *Xanthomonas*
482 effector XopL uncovers the role of microtubules in stromule extension and
483 dynamics in *Nicotiana benthamiana*. *Plant J* **93**:856–870. doi:10.1111/tpj.13813
- 484 Gibson DG, Young L, Chuang R-Y, Venter JC, Hutchison CA, Smith HO. 2009.
485 Enzymatic assembly of DNA molecules up to several hundred kilobases. *Nat*
486 *Methods* **6**:343–5. doi:10.1038/nmeth.1318
- 487 Hanson MR, Hines KM. 2017. Stromules: Probing Formation and Function. *Plant Physiol*
488 **176**:pp.01287.2017. doi:10.1104/pp.17.01287

- 489 Hawes C. 2018. The Plant Endoplasmic Reticulum, *Methods in Molecular Biology*. New
490 York, NY: Springer New York. doi:10.1007/978-1-4939-7389-7
- 491 Hellens R, Mullineaux P, Klee H. 2000. Technical Focus:a guide to Agrobacterium binary
492 Ti vectors. *Trends Plant Sci* **5**:446–51.
- 493 Helliwell C, Waterhouse P. 2003. Constructs and methods for high-throughput gene
494 silencing in plants. *Methods* **30**:289–95.
- 495 Hoitzing H, Johnston IG, Jones NS. 2015. What is the function of mitochondrial
496 networks? A theoretical assessment of hypotheses and proposal for future
497 research. *BioEssays* **37**:687–700. doi:10.1002/bies.201400188
- 498 Jelenska J, Yao N, Vinatzer BA, Wright CM, Brodsky JL, Greenberg JT. 2007. A J
499 Domain Virulence Effector of *Pseudomonas syringae* Remodels Host Chloroplasts
500 and Suppresses Defenses. *Curr Biol* **17**:499–508. doi:10.1016/j.cub.2007.02.028
- 501 Kadota A, Yamada N, Suetsugu N, Hirose M, Saito C, Shoda K, Ichikawa S, Kagawa T,
502 Nakano A, Wada M. 2009. Short actin-based mechanism for light-directed
503 chloroplast movement in *Arabidopsis*. *Proc Natl Acad Sci* **106**:13106–13111.
504 doi:10.1073/pnas.0906250106
- 505 Karimi M, Inzé D, Depicker A. 2002. GATEWAY vectors for Agrobacterium-mediated
506 plant transformation. *Trends Plant Sci* **7**:193–5. doi:10.1016/S1360-1385(02)02251-
507 3
- 508 Kasahara M, Kagawa T, Oikawa K, Suetsugu N, Miyao M, Wada M. 2002. Chloroplast
509 avoidance movement reduces photodamage in plants. *Nature* **420**:829–832.
510 doi:10.1038/nature01213
- 511 Koh S, André A, Edwards H, Ehrhardt D, Somerville S. 2005. *Arabidopsis thaliana*
512 subcellular responses to compatible *Erysiphe cichoracearum* infections. *Plant J*
513 **44**:516–529. doi:10.1111/j.1365-313X.2005.02545.x
- 514 Krenz B, Jeske H, Kleinow T. 2012. The induction of stromule formation by a plant DNA-

515 virus in epidermal leaf tissues suggests a novel intra- and intercellular
516 macromolecular trafficking route. *Front Plant Sci* **3**:1–12.
517 doi:10.3389/fpls.2012.00291

518 Kumar AS, Park E, Nedo A, Alqarni A, Ren L, Hoban K, Modla S, McDonald JH,
519 Kambhamettu C, Dinesh-Kumar SP, Caplan JL. 2018. Stromule extension along
520 microtubules coordinated with actin-mediated anchoring guides perinuclear
521 chloroplast movement during innate immunity. *Elife* **7**:1–33.
522 doi:10.7554/eLife.23625

523 Kwon C, Neu C, Pajonk S, Yun HS, Lipka U, Humphry M, Bau S, Straus M, Kwaaitaal M,
524 Rampelt H, El Kasmi F, Jürgens G, Parker J, Panstruga R, Lipka V, Schulze-Lefert
525 P. 2008. Co-option of a default secretory pathway for plant immune responses.
526 *Nature* **451**:835–40. doi:10.1038/nature06545

527 Oikawa K, Kasahara M, Kiyosue T, Kagawa T, Suetsugu N, Takahashi F, Kanegae T,
528 Niwa Y, Kadota A, Wada M. 2003. Chloroplast unusual positioning1 is essential for
529 proper chloroplast positioning. *Plant Cell* **15**:2805–15. doi:10.1105/tpc.016428

530 Oikawa K, Yamasato A, Kong S-G, Kasahara M, Nakai M, Takahashi F, Ogura Y,
531 Kagawa T, Wada M. 2008. Chloroplast Outer Envelope Protein CHUP1 Is Essential
532 for Chloroplast Anchorage to the Plasma Membrane and Chloroplast Movement.
533 *Plant Physiol* **148**:829–842. doi:10.1104/pp.108.123075

534 Padmanabhan MS, Dinesh-Kumar SP. 2010. All Hands on Deck—The Role of
535 Chloroplasts, Endoplasmic Reticulum, and the Nucleus in Driving Plant Innate
536 Immunity. *Mol Plant-Microbe Interact* **23**:1368–1380. doi:10.1094/MPMI-05-10-0113

537 Pecrix Y, Buendia L, Penouilh-Suzette C, Maréchaux M, Legrand L, Bouchez O, Rengel
538 D, Gouzy J, Cottret L, Vear F, Godiard L. 2018. Sunflower resistance to multiple
539 downy mildew pathotypes revealed by recognition of conserved effectors of the
540 oomycete *Plasmopara halstedii*. *Plant J*. doi:10.1111/tpj.14157

- 541 Perraki A, DeFalco TA, Derbyshire P, Avila J, Séré D, Sklenar J, Qi X, Stransfeld L,
542 Schwessinger B, Kadota Y, Macho AP, Jiang S, Couto D, Torii KU, Menke FLH,
543 Zipfel C. 2018. Phosphocode-dependent functional dichotomy of a common co-
544 receptor in plant signalling. *Nature* **561**:248–252. doi:10.1038/s41586-018-0471-x
- 545 Petre B, Lorrain C, Saunders DGO, Win J, Sklenar J, Duplessis S, Kamoun S. 2016.
546 Rust fungal effectors mimic host transit peptides to translocate into chloroplasts.
547 *Cell Microbiol* **18**:453–465. doi:10.1111/cmi.12530
- 548 Saunders DGO, Breen S, Win J, Schornack S, Hein I, Bozkurt TO, Champouret N,
549 Vleeshouwers VG a a, Birch PRJ, Gilroy EM, Kamoun S. 2012. Host protein BSL1
550 associates with *Phytophthora infestans* RXLR effector AVR2 and the *Solanum*
551 *demissum* Immune receptor R2 to mediate disease resistance. *Plant Cell* **24**:3420–
552 34. doi:10.1105/tpc.112.099861
- 553 Schattat MH, Barton KA, Mathur J. 2014. The myth of interconnected plastids and
554 related phenomena. *Protoplasma* **252**:359–371. doi:10.1007/s00709-014-0666-4
- 555 Serrano I, Audran C, Rivas S. 2016. Chloroplasts at work during plant innate immunity. *J*
556 *Exp Bot* **67**:3845–3854. doi:10.1093/jxb/erw088
- 557 Smakowska-Luzan E, Mott GA, Parys K, Stegmann M, Howton TC, Layeghifard M,
558 Neuhold J, Lehner A, Kong J, Grünwald K, Weinberger N, Satbhai SB, Mayer D,
559 Busch W, Madalinski M, Stolt-Bergner P, Provarnt NJ, Mukhtar MS, Zipfel C,
560 Desveaux D, Guttman DS, Belkhadir Y. 2018. An extracellular network of
561 *Arabidopsis* leucine-rich repeat receptor kinases. *Nature* **553**:342–346.
562 doi:10.1038/nature25184
- 563 Song J, Win J, Tian M, Schornack S, Kaschani F, Ilyas M, Hoorn RAL Van Der, Kamoun
564 S. 2009. Apoplastic effectors secreted by two unrelated eukaryotic plant pathogens
565 target the tomato defense protease Rcr3.
- 566 Stegemann S, Keuthe M, Greiner S, Bock R. 2012. Horizontal transfer of chloroplast

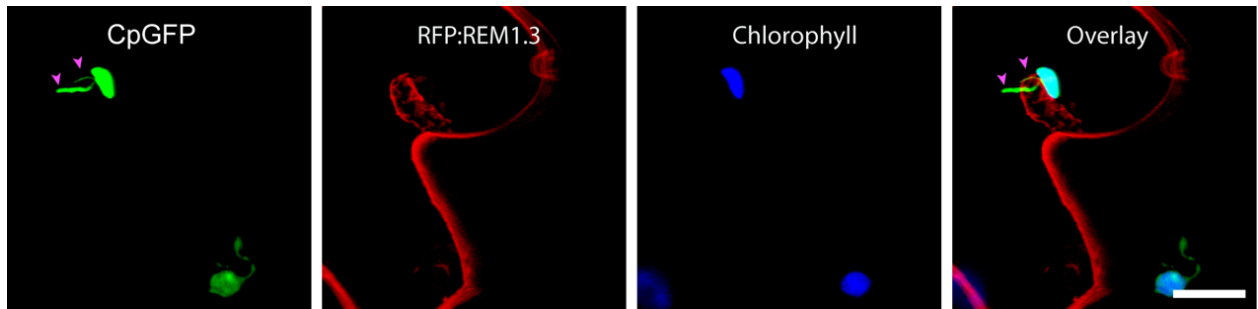
- 567 genomes between plant species. *Proc Natl Acad Sci* **109**:2434–2438.
568 doi:10.1073/pnas.1114076109
- 569 Su J, Yang L, Zhu Q, Wu H, He Y, Liu Y, Xu J, Jiang D, Zhang S. 2018. Active
570 photosynthetic inhibition mediated by MPK3/MPK6 is critical to effector-triggered
571 immunity. *PLoS Biol* **16**:1–29. doi:10.1371/journal.pbio.2004122
- 572 Trotta A, Rahikainen M, Konert G, Finazzi G, Kangasjärvi S. 2014. Signalling crosstalk in
573 light stress and immune reactions in plants. *Philos Trans R Soc Lond B Biol Sci*
574 **369**:20130235. doi:10.1098/rstb.2013.0235
- 575 van Damme M, Zeilmaker T, Elberse J, Andel A, de Sain-van der Velden M, van den
576 Ackerveken G. 2009. Downy Mildew Resistance in Arabidopsis by Mutation of
577 HOMOSERINE KINASE. *Plant Cell Online* **21**:2179–2189.
578 doi:10.1105/tpc.109.066811
- 579 Van West P, De Jong AJ, Judelson HS, Emons AMC, Govers F. 1998. The ipiO gene of
580 phytophthora infestans is highly expressed in invading hyphae during infection.
581 *Fungal Genet Biol* **23**:126–138. doi:10.1006/fgbi.1998.1036
- 582 Wang S, Boevink PC, Welsh L, Zhang R, Whisson SC, Birch PRJ. 2017. Delivery of
583 cytoplasmic and apoplastic effectors from *Phytophthora infestans* haustoria by
584 distinct secretion pathways. *New Phytol*. doi:10.1111/nph.14696
- 585 Whisson SC, Boevink PC, Moleleki L, Avrova AO, Morales JG, Gilroy EM, Armstrong
586 MR, Grouffaud S, Van West P, Chapman S, Hein I, Toth IK, Pritchard L, Birch PRJ.
587 2007. A translocation signal for delivery of oomycete effector proteins into host
588 plant cells. *Nature* **450**:115–118. doi:10.1038/nature06203
- 589 Whisson SC, Boevink PC, Wang S, Birch PR. 2016. The cell biology of late blight
590 disease. *Curr Opin Microbiol* **34**:127–135. doi:10.1016/j.mib.2016.09.002
591

592 **List of Supplementary Materials:**

593 Figures S1-S9

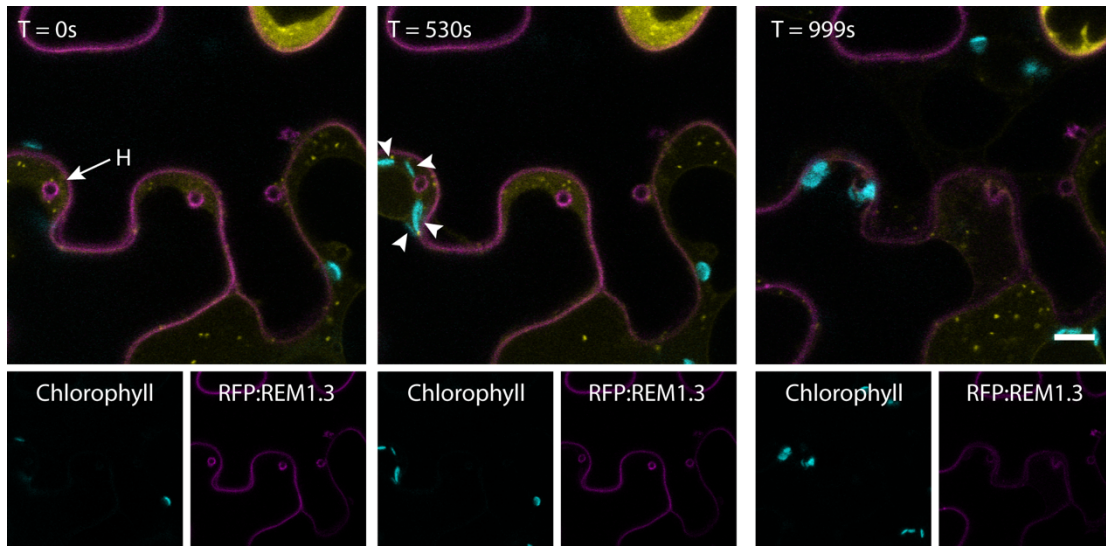
594 Table S1

595 Movies S1-S13



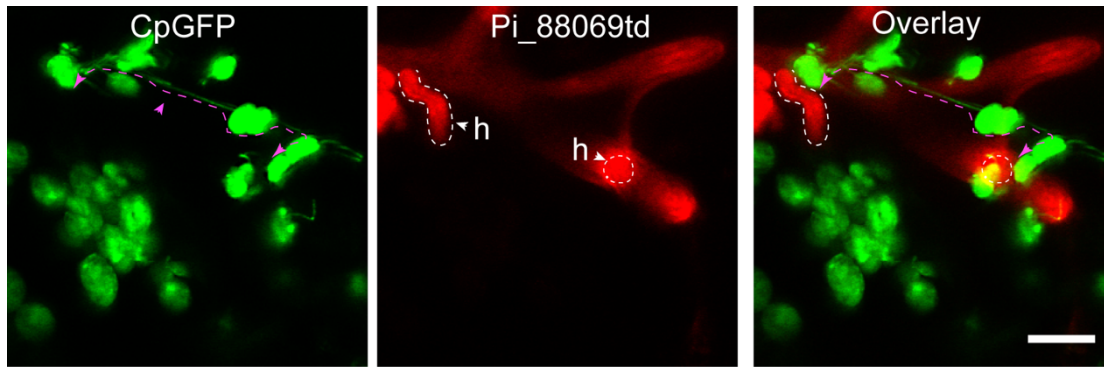
596

597 **Fig. S1: Confocal micrographs showing a chloroplast embracing a haustorium**
598 **with its stromules.** Leaf epidermal cells from transplastomic CpGFP *N. benthamiana*
599 plants transiently expressing plasma membrane and EHM marker RFP:REM1.3 were
600 infected with WT *P. infestans* 8806 and imaged 4dpi. Blue represents chlorophyll
601 autofluorescence. Scale bar is 10 μ m. Magenta arrowheads indicate stromules.



602
603

604 **Fig. S2: Time-lapse series showing chloroplasts accumulation towards a**
605 **haustorium.** Leaf epidermal cells from WT *N. benthamiana* plants expressing PM and
606 EHM marker RFP:REM1.3 (Magenta) and endosomal marker GFP:RAB8 (Yellow)
607 infected with WT *P. infestans* 88069. Cyan is chlorophyll autofluorescence, labelling the
608 chloroplasts. Scale bar is 10 μ m.



609

610

611

612 **Fig. S3: Chloroplasts form long-distance stromule interactions that can bridge**

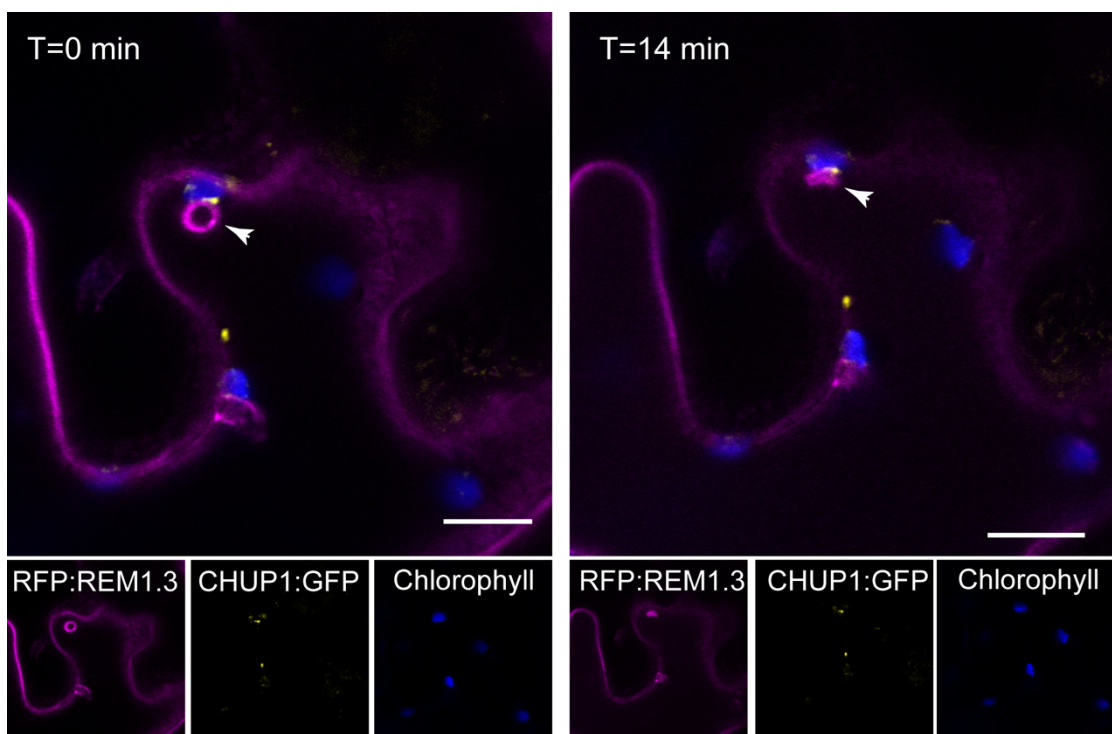
613 **more than one haustorium.** Confocal micrographs of leaf epidermal cells from

614 transplastomic CpGFP *N. benthamiana* plants. Maximum intensity projection (10

615 images), 5 dpi (days post infection) with red-fluorescent *P. infestans* strain 88069td. 'h'

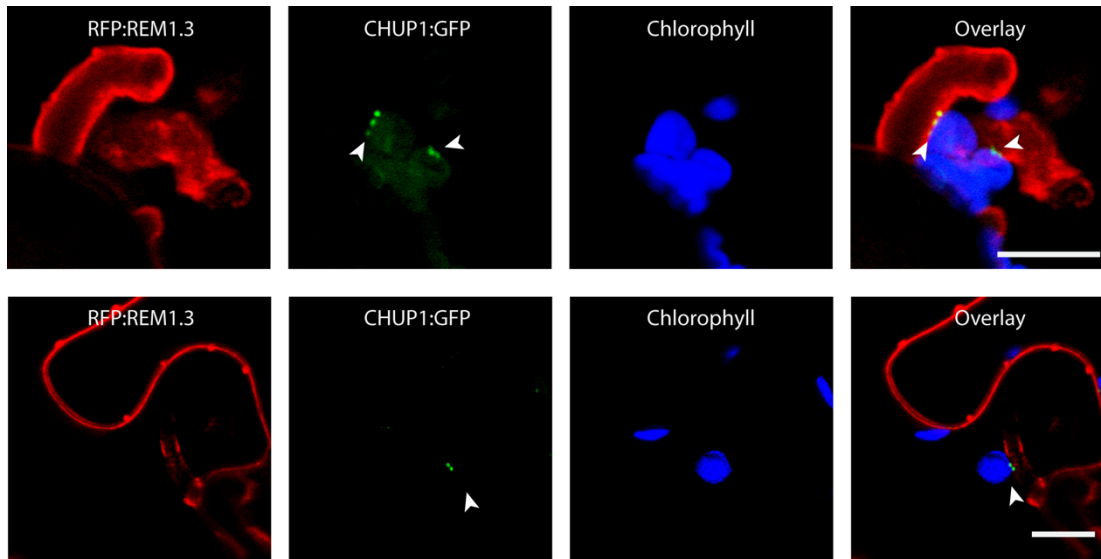
616 indicates haustorium, Magenta arrowheads indicate long-distance stromule interactions.

Scale bars are 10 μ m. See 3D Movie 7.



617
618
619
620
621

Fig. S4: Time-lapse series showing collapse of haustorium. *N. benthamiana* leaves transiently co-expressing plasma membrane and EHM marker RFP:REM1.3 with CHUP1:GFP. Arrowhead indicates haustorium that collapses. Scale bars are 10 μ m.



622

623

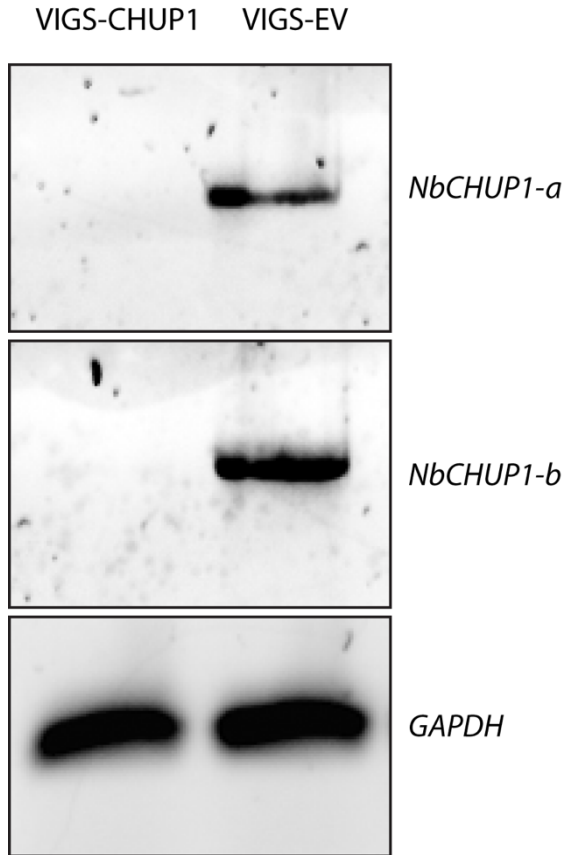
624

625 **Fig. S5: CHUP1:GFP accumulates at the contact points between the chloroplast**

626 **and the EHM.** *N. benthamiana* leaves transiently co-expressing plasma membrane and

627 EHM marker RFP:REM1.3 with CHUP1:GFP were infected with WT *P. infestans* 88069.

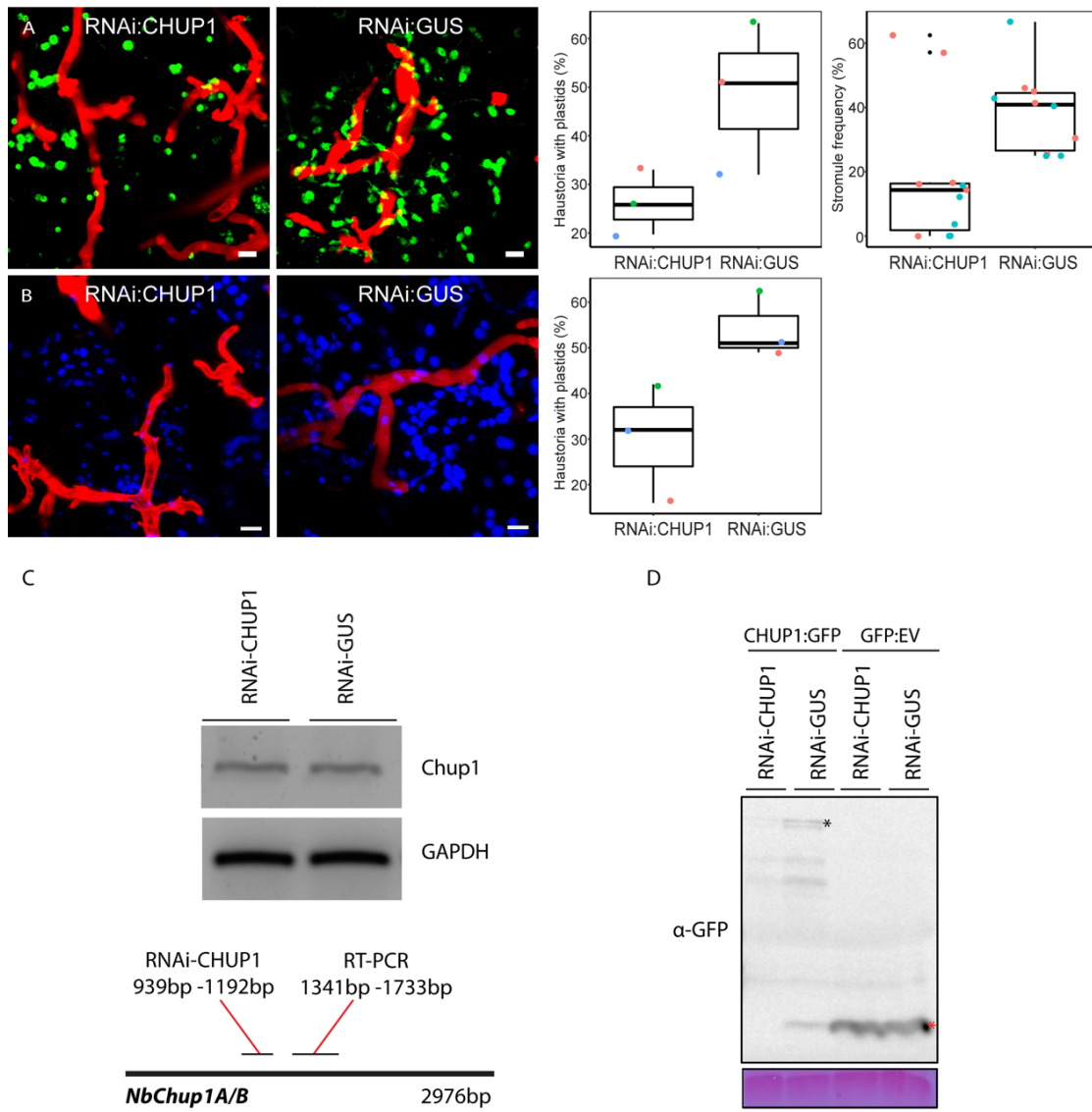
Blue represents chlorophyll autofluorescence. Scale bars are 10 μ m.



RT-PCR (Full-length) (2436bp-2935bp)
NbChup1A/B 2976bp

628
629

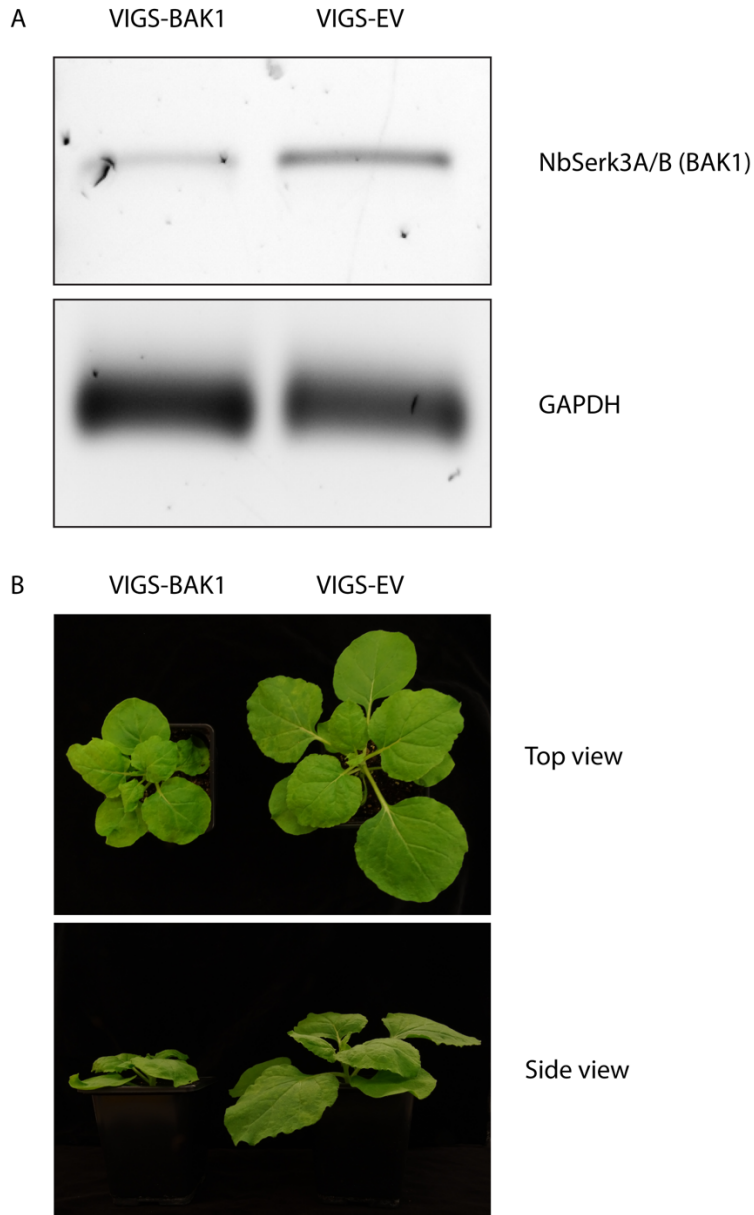
630 **Fig. S6: VIGS-CHUP1 silences CHUP1 compared to the EV control.** 12 day old
631 transplastomic CpGFP *N. benthamiana* plants, were infiltrated with *Agrobacterium*
632 expressing TRV2:CHUP1 or TRV2:EV. Leaf disks were taken from 5-week old,
633 uninfected, silenced tissue and RNA was extracted. Semi-quantitative RT-PCR of
634 *CHUP1* shows that it was silenced in VIGS-CHUP1 tissue compared to EV. RT-PCR of
635 housekeeping *GAPDH* was used as an internal control for cDNA loading. For both,
636 primers that did not amplify the silencing target were use



637

638 **Fig. S7: RNAi of CHUP1 suppresses stromule formation and haustorial**
 639 **accumulation of chloroplasts (A)** Confocal micrographs of leaf epidermal cells from
 640 transplastomic CpGFP *N. benthamiana* plants, in which *CHUP1* is locally silenced
 641 (RNAi-CHUP1), 5-7 dpi with *P. infestans* (88069td), with RNAi-GUS included as a
 642 control. The first scatter-boxplot depicts the effect of RNAi-CHUP1 silencing on the
 643 percentage of haustoria in contact with at least one plastid (27% of $n = 237$ haustoria),
 644 compared to RNAi-GUS control (50% of $n = 126$ haustoria) ($p < 0.01$). The second
 645 scatter boxplot depicts the effect of RNAi-CHUP1 silencing on the percentage of

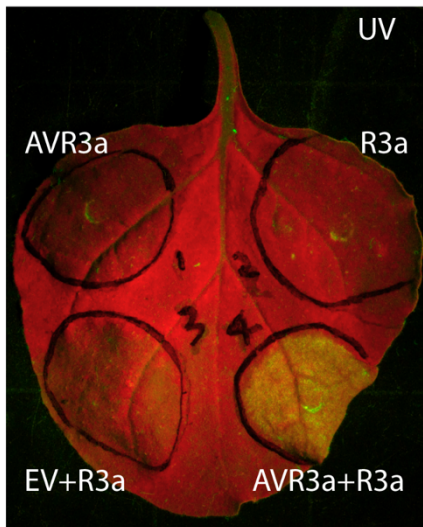
646 chloroplasts with one (or more) stromule(s) (18%, $n = 11$ images quantified) compared to
647 RNAi-GUS control (39%, $n = 10$ images quantified) ($p < 0.05$). (B) Confocal micrographs
648 of leaf epidermal cells from WT *N. benthamiana* plants, in which *CHUP1* is locally
649 silenced (RNAi-CHUP1), 5-7 dpi with *P. infestans* (88069td), with RNAi-GUS included as
650 a control. The scatter-boxplot depicts the effect of RNAi-CHUP1 silencing on the
651 percentage of haustoria in contact with at least one plastid (30% of $n = 392$ haustoria),
652 compared to RNAi-GUS control (55% of $n = 215$ haustoria) ($p < 0.01$). Scale bars are 10
653 μm . (C) Leaf disks were taken from uninfected tissue infiltrated to express the RNAi
654 construct at 6 days post infiltration and RNA was extracted. Following semi-quantitative
655 RT-PCR of *CHUP1* we noted only a slight reduction of *CHUP1* mRNA from RNAi-
656 CHUP1 tissue compared to RNAi-GUS control. However, clear silencing of CHUP1:GFP
657 was seen upon western blotting (D), indicating that the RNAi-CHUP1 hairpin silencing
658 construct mainly acts by blocking CHUP1 translation, as is known to occur for in
659 RNAi(Brodersen et al., 2008).



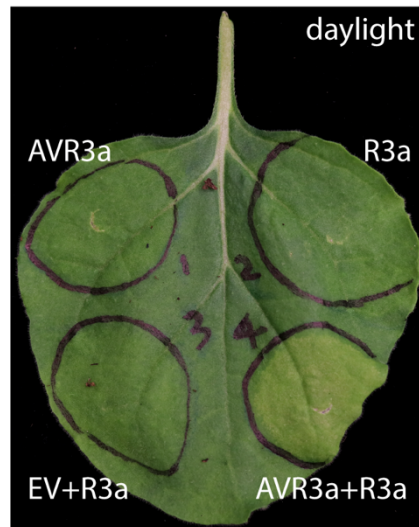
660

661 **Fig. S8: VIGS-BAK1 silences BAK1 compared to the EV control.** 12 day old
662 transplastomic CpGFP *N. benthamiana* plants, were infiltrated with *Agrobacterium*
663 expressing TRV2:BAK1 or TRV2:EV. (A) Leaf disks were taken from uninfected,
664 silenced tissue and RNA was extracted. Semi-quantitative RT-PCR of *BAK1* shows that
665 it was silenced in VIGS-BAK1 tissue compared to EV. RT-PCR of housekeeping GAPDH
666 was used as an internal control for cDNA loading. For both, primers that did not amplify
667 the silencing target were used. (B) Photos of representative *N. benthamiana* plants 5
668 weeks old, showing symptoms of *BAK1* silencing by VIGS.

A



B



669
670
671
672
673

Fig. S9: AVR3a expression triggers HR in an R3a-dependent manner, indicating it is functional. AVR3a or R3a were expressed alone, triggering no HR. EV and R3a also triggered no HR. Only expression of AVR3a with R3a triggered HR, as visible by white light or autofluorescence under UV light.

674 **Table S1. Primers used in this study**

Primer name	Sequence (5' to 3')
CHUP1-A F	AGGCGGCCGCACTAGTATGATAGTCAGGGTAGGTTTAGTG G
GA_CHUP1_R1	GTTCCAAAAGTGTGATGGCTAC
GA_CHUP1B_F2	GCTCAGAAATGCAGGTGATGGT
GA_CHUP1B_R 2	TCCTCGCCCTTGCTCACCATTGATCCTGTTTCTTGTGTATTC TCTTCTCC
VIGS-_CHUP1_F	GGTTGATGAACGAGCTGTCCTCAAG
VIGS_CHUP1_R 2	TGACACGACTCCTTAATTCTTCAAAG
CHP1_RT_F1	ATGATAGTCAGGGTAGGTTTAGTG
BD-CHUP1-REV	ACCAGGTCTCACACCTTGTTCTTGTGTA CTCTCT
CHUP1a_RT_F	ATGATCGTCAGGGTAGGTTTAGTGGTTGC
CHUP1a_RT_R	TGTTTCTTGTGTATTCTCTTCTCCTGTTTGT
CHUP1b_RT_F	ATGATAGTCAGGGTAGGTTTAGTGGTTGC
CHUP1b_RT_R	TGTTTCTTGTGTATTCTCTTCTCCTGTTTGT

675

676 **Movie S1: 3D image of Fig. 1A showing chloroplast focal accumulation at**
677 **haustoria and stromules interacting with each other and other chloroplasts.** 3D
678 visualisation comprises Z-stack of confocal images of leaf epidermal cells from
679 transplastomic CpGFP (Yellow) *N. benthamiana* plants infected with red-fluorescent *P.*
680 *infestans* strain 88069td (Magenta).

681 **Movie S2: 3D time-lapse series showing chloroplasts sieging haustoria.** 3D
682 visualisation comprises Z-stack of confocal images of leaf epidermal cells from
683 transplastomic CpGFP (Yellow) *N. benthamiana* plants infected with red-fluorescent *P.*
684 *infestans* strain 88069td (Magenta).

685 **Movie S3: 3D time-lapse series showing stromules engulfing a haustorium.** 3D
686 visualisation comprises Z-stack of confocal images of leaf epidermal cells from
687 transplastomic CpGFP (Yellow) *N. benthamiana* plants infected with red-fluorescent *P.*
688 *infestans* strain 88069td (Magenta). Grayscale crop of CpGFP signal highlights the
689 extent of chloroplast stromules embracing the haustorium.

690 **Movie S4: 3D image of chloroplast and stromules embracing a haustorium.** 3D
691 visualisation comprises Z-stack of confocal images of leaf epidermal cells from
692 transplastomic CpGFP (Yellow) *N. benthamiana* plants expressing PM and EHM marker
693 RFP:REM1.3 (Magenta) infected with WT *P. infestans* 88069.

694 **Movie S5: Time-lapse series of Fig. S1 showing chloroplasts accumulation to a**
695 **haustorium.** Leaf epidermal cells from WT *N. benthamiana* plants expressing PM and
696 EHM marker RFP:REM1.3 (Magenta) and endosomal marker GFP:RAB8 (Yellow)
697 infected with WT *P. infestans* 88069. Blue is chlorophyll autofluorescence, labelling the
698 chloroplasts.

699 **Movie S6: Time-lapse series showing optical trapping of chloroplast in Fig. 1G**
700 **which escapes the trap and springs back to the haustorium.** TIRF microscopy
701 combined with laser capture in leaf epidermal cells from transplastomic CpGFP (channel
702 not shown) *N. benthamiana* plants expressing PM and EHM marker RFP:REM1.3
703 (Grayscale) infected with WT *P. infestans* 88069. Chloroplast is visible due to chlorophyll
704 autofluorescence overlapping with RFP emission spectrum. Scale bar is 10 µm.

705 **Movie S7: 3D image of Fig. S3 showing chloroplasts form long-distance stromule**
706 **interactions that can bridge more than one haustorium.** 3D visualisation comprises
707 Z-stack of confocal images of leaf epidermal cells from transplastomic CpGFP (Yellow)
708 *N. benthamiana* plants infected with red-fluorescent *P. infestans* strain 88069td
709 (Magenta). 'H' indicates haustorium.

710 **Movie S8: 3D time-lapse series showing dynamic stromule interactions.** 3D
711 visualisation comprises Z-stack of confocal images of leaf epidermal cells from
712 transplastomic CpGFP (Yellow) *N. benthamiana* plants infected with red-fluorescent *P.*
713 *infestans* strain 88069td (Magenta).

714 **Movie S9: Time-lapse series showing optical trapping of chloroplast in Fig. 1H and**
715 **comigration of a second chloroplast interacting via a stromule-like extension.**
716 TIRF microscopy combined with laser capture in leaf epidermal cells from transplastomic
717 CpGFP (Grayscale) *N. benthamiana* plants. Scale bar is 10 µm.

718

719 **Movie S10: Time-lapse series of Fig. S3 showing collapse of haustorium engulfed**
720 **by a chloroplast.** Leaf epidermal cells from WT *N. benthamiana* plants expressing
721 CHUP1:GFP (Yellow) and PM and EHM marker RFP:REM1.3 (Magenta) infected with
722 WT *P. infestans* 88069. Blue is chlorophyll autofluorescence, labelling the chloroplasts.
723 “H” indicates haustorium that collapses.

724 **Movie S11: Time-lapse series of Fig. S3 showing collapse of haustorium**
725 **associated with a chloroplast.** Leaf epidermal cells from WT *N. benthamiana* plants
726 expressing PM and EHM marker RFP:REM1.3 (Magenta) and endosomal marker
727 GFP:RAB8 (Yellow) infected with WT *P. infestans* 88069. Blue is chlorophyll
728 autofluorescence, labelling the chloroplasts. “H” indicates haustorium that collapses.

729 **Movie S12: Time-lapse series showing synchronised steering of chloroplasts**
730 **away from haustorium.** Leaf epidermal cells from transplastomic CpGFP (Yellow) *N.*
731 *benthamiana* plants expressing PM and EHM marker RFP:REM1.3 (Magenta) and GFP-
732 NbNRC2 (NLR, channel not shown) infected with WT *P. infestans* 88069.

733 **Movie S13: Time-lapse series showing chloroplasts synchronised in pulling away**
734 **from haustorium.** Leaf epidermal cells from transplastomic CpGFP (Yellow) *N.*
735 *benthamiana* plants expressing PM and EHM marker RFP:REM1.3 (Magenta) infected
736 with WT *P. infestans* 88069. “H” indicates haustorium the chloroplasts pull away from in
737 a synchronised manner.